ADVANCED MATERIALS
www.advmat.de

www.MaterialsViews.com

Epitaxial Growth of Intermetallic MnPt Films on Oxides and Large Exchange Bias

Zhiqi Liu, Michael D. Biegalski, Shang-Lin Hsu, Shunli Shang, Cassie Marker, Jian Liu, Li Li, Lisha Fan, Tricia L. Meyer, Anthony T. Wong, John A. Nichols, Deyang Chen, Long You, Zuhuang Chen, Kai Wang, Kevin Wang, Thomas Z. Ward, Zheng Gai, Ho Nyung Lee, Athena S. Sefat, Valeria Lauter, Zi-Kui Liu, and Hans M. Christen**

We dedicate this work to the deceased Dr. Michael D. Biegalski

Electrical control of magnetism in multiferroic materials and heterostructures is promising for low-energy spintronic and information storage devices.[1] Recently, multiferroic heterostructures consisting of epitaxial intermetallic alloys with multiple magnetic phases and functional ferroelectric oxides have shown giant magnetoelectric (ME) coupling and accordingly large potential for information storage devices.[2,3] Specifically, electrical switching between ferromagnetic (FM) and antiferromagnetic (AFM) order was achieved[2] by combining intermetallic alloy FeRh with ferroelectric $BaTiO_3$. The ME coupling coefficient reached 1.6×10^{-5} s m^{-1}, one or two orders of magnitude higher than previous reports[4,5] in multiferroic heterostructures. In our previous work, a large reversible electroresistance of 8% was obtained for metallic FeRh in epitaxial FeRh/PMN-PT ($0.72PbMg_{1/3}Nb_{2/3}O_3$–$0.28PbTiO_3$) heterostructures, via strain-mediated ME coupling and the resulting magnetic phase switching.[3]

$Mn_{50}Pt_{50}$ is a traditional AFM intermetallic alloy with a very high Néel temperature $T_N \approx 973$ K.[6] It has a CuAu-I ($L1_0$) type tetragonal crystal structure with lattice parameters $a = 2.827$ Å, $c = 3.669$ Å, and, accordingly, the tetragonality $c/\sqrt{2}a = 0.918$. The tetragonal phase is stable with Pt composition between 33 and 60 at%.[7] Depending on the Pt composition, the Néel temperature and lattice parameters can be largely varied. In addition to its robust AFM order in bulk, it has a spin-flip transition driven by the *c*-axis contraction in highly ordered single crystals, where the spin axis changes from the *c*-axis to within the *c*-plane upon heating across the transition temperature.[6,8] Such a strongly structure–magnetism correlated system is indeed an ideal candidate for the electrical control of spin structure via strain-mediated ME coupling, provided that highly ordered single-crystal MnPt films could be successfully integrated on proper functional oxides. On the other hand, the relativistic spin–orbit coupling of the AFM alloys makes it highly applicable to AFM spintronics.[9–12] For example, AFM intermetallic alloys have been utilized in AFM-based tunneling junctions;[10,13] and epitaxial AFM intermetallic films grown on oxides were recently explored to be a new type of AFM memory resistor based on anisotropic magnetoresistance which exhibited superior stray field insensitivity.[14]

As an AFM material, amorphous and polycrystalline MnPt films were mainly fabricated at low temperatures on metal layers

Dr. Z. Q. Liu,[+] Dr. M. D. Biegalski, Dr. K. Wang, Dr. Z. Gai, Dr. H. M. Christen
Center for Nanophase Materials Sciences
Oak Ridge National Laboratory
Oak Ridge, TN 37831, USA
E-mail: liuzhiqi@berkeley.edu; christenhm@ornl.gov

S.-L. Hsu, Dr. J. Liu, D. Y. Chen, Dr. Z. H. Chen, K. Wang
Department of Materials Science and Engineering
University of California
Berkeley, CA 94720, USA

S.-L. Hsu, Dr. J. Liu
Materials Sciences Division
Lawrence Berkeley National Laboratory
Berkeley, CA 94720, USA

Dr. S. L. Shang, C. Marker, Prof. Z. K. Liu
Department of Materials Science and Engineering
The Pennsylvania State University
University Park, PA 16802, USA

Dr. J. Liu
Department of Physics
University of California
Berkeley, CA 94720, USA

Dr. L. Li, Dr. L. S. Fan, Dr. T. L. Meyer, A. T. Wong, Dr. J. A. Nichols, Dr. T. Z. Ward, Dr. H. N. Lee, Dr. A. S. Sefat
Materials Science and Technology Division
Oak Ridge National Laboratory
Oak Ridge, TN 37831, USA

A. T. Wong
Materials Science and Engineering
University of Tennessee
Knoxville, TN 37996, USA

Dr. L. You
Department of Electrical Engineering and Computer Science
University of California
Berkeley, CA 94720, USA

Dr. V. Lauter
Spallation Neutron Source
Oak Ridge National Laboratory
Oak Ridge, TN 37831, USA

[+]Present address: Department of Materials Science and Engineering, University of California, Berkeley, CA 94720, USA

DOI: 10.1002/adma.201502606

for exchange bias in spin valve devices and other studies,[15–19] where the exchange coupling between AFM MnPt and a ferromagnetic layer is closely related to chemical ordering of MnPt. Epitaxial growth of intermetallic alloys on oxides is, however, much more challenging. The reasons are 1) epitaxy of intermetallic alloys typically needs high thermal energy during growth so that atoms are sufficiently energetic to move into ordered lattice points, thus experimentally demanding a high growth temperature; 2) most intermetallic alloys are rather chemically reactive at high temperatures and hence chemical interactions can often occur at interfaces between alloy films and oxides including oxidation and re-alloying; 3) the interfacial wetting issue of metal films on oxides due to the large difference in surface energy can prevent epitaxial growth of intermetallic films; 4) unlike the epitaxy of oxide films on oxide substrates that are capable of accommodating large epitaxial strain, metal films are much more difficult to be strained as a result of their significantly distinct mechanical properties compared with oxides,[20] and therefore even a small lattice mismatch between substrates and metal films may disrupt epitaxy, leading to textured or polycrystalline growth.

Therefore, one needs to start with oxide substrates not only with in-plane lattice parameters close to those of MnPt but also chemically inert to metal alloys at high temperatures. For example, $SrTiO_3$ and $BaTiO_3$ may not be ideal for sharp interfaces in this case although their lattice parameters (a = 3.905 Å for $SrTiO_3$ and a = 4.000 Å for $BaTiO_3$ above 120 °C) are relatively close to $\sqrt{2}a$ = 4.002 Å (considering 45° in-plane rotation relative to oxide substrates) of MnPt. Due to the large oxygen diffusivity in titanates, their surfaces can be remarkably reduced in vacuum at high temperatures[21,22] or even by room-temperature deposition of chemically reactive elements on top,[23] which would induce heavy interfacial oxidation in metal alloys. Here, we report successful epitaxial growth of MnPt films on spinel $MgAl_2O_4$ (MAO) substrates and their electrical and magnetic properties. The interface between MnPt and MAO is remarkably sharp for a metal/oxide interface. Moreover, as-grown films are found to be ferromagnetic by superconducting quantum interference device (SQUID) and polarized neutron reflectometry (PNR) measurements. A subsequent high-temperature anneal is shown to allow for recovery of a bulk-like AFM behavior while maintain excellent epitaxy to substrate.

MAO is stable at room temperature and high temperatures with a melting point of 2135 °C. It is robust to many acids and alkalis. It has a cubic spinel structure with a = 8.083 Å,[24] half of which is close to the in-plane lattice parameter of MnPt. Accordingly, MnPt films were deposited from a nominal $Mn_{50}Pt_{50}$ target on the (001)-oriented MAO substrates at 600 °C in a radio frequency sputtering system equipped with reflection high-energy electron diffraction (RHEED) and a laser heater. The base pressure was 2×10^{-7} Torr. The ramping rate was kept at 10 °C min^{-1} during both heating and cooling. The composition of thin films depends on sputtering power and Ar gas pressure owing to different yields of Mn and Pt elements, which was measured by Rutherford backscattering spectrometry (RBS) in University of California, Berkeley and scanning electron microscopy with energy-dispersive X-ray spectroscopy (SEM-EDS) in our institute. The sputtering power and Ar pressure were optimized to be 60 W and 5 mTorr, respectively, giving rise to $Mn_{46}Pt_{54}$ (±2 at%) films. In addition, the deposition rate was determined to be 0.33 Å s^{-1} by X-ray reflectivity (XRR) measurements.

Figure 1a,b shows the RHEED patterns of a (001)-oriented MAO substrate at 600 °C and 5 mTorr Ar pressure before deposition along in-plane [100] and [110] directions, respectively, which reveal high surface crystallinity of the MAO substrate. The initial growth of MnPt on MAO was observed to be in the 3D island growth mode, corresponding to a square-lattice diffraction pattern. After the initial 4 nm growth, the RHEED pattern becomes streaky. Beyond a 20 nm thickness, pattern intensity begins to decrease, which signals the onset of surface degradation. The RHEED patterns of a 20 nm thick MnPt film are shown in Figure 1c,d. Regarding the growth of a metal film on an oxide substrate, layer-by-layer growth leading to a film surface with the same smoothness as the substrate typically does not occur while oriented and coalesced island formation,

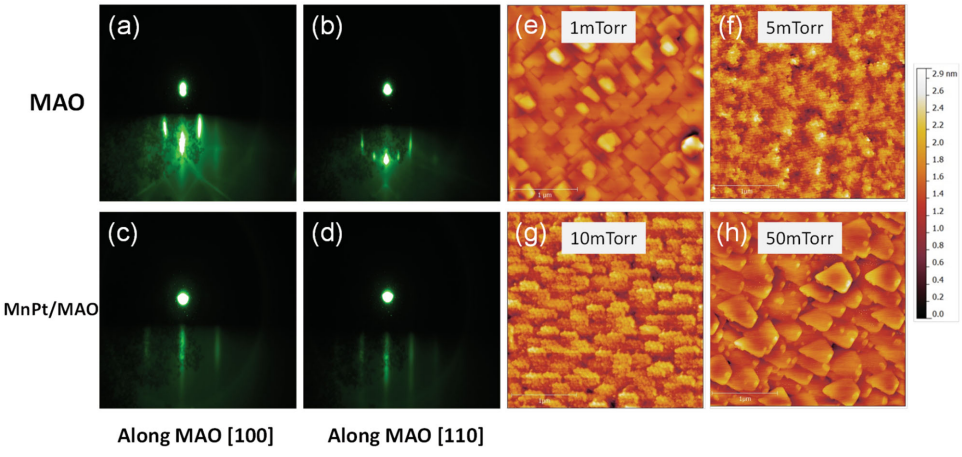

Figure 1. RHEED patterns and atomic force microscopy images. RHEED patterns of an MAO substrate at 600 °C along the a) [100] and b) [110] directions. RHEED patterns of a 20 nm thick MnPt film grown on MAO at 600 °C and 5 mTorr Ar pressure along the c) [100] and d) [110] directions. Note: the dark feature within the RHEED pattern was due to the undesired metal coating on the RHEED screen. e–h) AFM images of MnPt films deposited at 600 °C and different Ar pressures.

ADVANCED MATERIALS
www.advmat.de

www.MaterialsViews.com

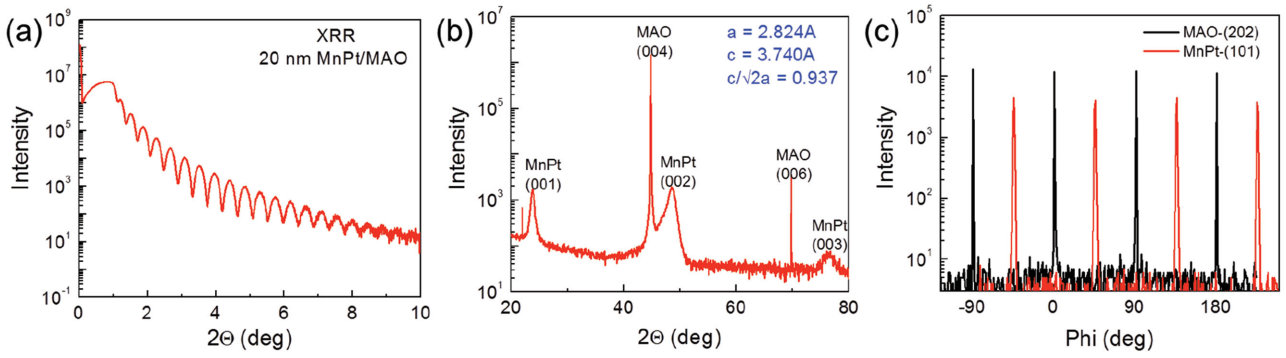

Figure 2. XRD characterization of a 20 nm thick MnPt/MAO film. a) XRR spectrum measured up to $2\theta = 10°$. b) θ–2θ scan from 20° to 80°. c) The 360° phi scans around the MnPt (101) peak and the MAO (202) peak.

such as in the atomic force microscopy images of 20 nm thick MnPt films deposited at 600 °C under different Ar pressures (Figure 1e–h), always occurs. An MnPt film deposited at 5 mTorr Ar pressure exhibits a minimal root mean square surface roughness of 0.33 nm and thus the pressure is fixed at 5 mTorr.

Figure 2a shows the XRR spectroscopy of an as-grown 20 nm MnPt/MAO heterostructure. Uniform thickness oscillations with a small damping effect can be clearly seen up to a high 2θ angle. This indicates a smooth and uniform film surface, which is consistent with the postgrowth RHEED patterns as shown in Figure 1. The out-of-plane θ–2θ X-ray diffraction (XRD) scan in Figure 2b reveals that the MnPt film is highly (001) oriented. The average out-of-plane lattice parameter was calculated to be $c = 3.740$ Å. The θ–2θ scan of the MnPt (101) peak further yielded the in-plane lattice parameter $a = 2.824$ Å. The tetragonality of the film is thus $c/\sqrt{2}a = 0.937$, which is quite close to that of bulk $Mn_{45}Pt_{55}$ alloy.[6] As seen in Figure 2c, 360° phi scans around the MAO (202) peak and the MnPt (101) peak both exhibit fourfold symmetry with 90° periodicity, pertaining to a square in-plane lattice. An in-plane rotation of 45° of the MnPt film relative to the MAO substrate is obvious from the 45° difference between two phi scans, which confirms epitaxy between films and substrates.

High-resolution cross-sectional transmission electron microscopy (TEM) analysis was performed in the scanning TEM (STEM) mode to further explore the structural and chemical properties of MnPt/MAO heterostructures. **Figure 3**a shows a cross-sectional TEM image of an as-grown MnPt/MAO heterostructure, where the MnPt lattice is epitaxial to MAO. Due to the *Z*-contrast function in the STEM mode and the large element mass contrast between MnPt and MAO, the underlying MAO substrate is heavily darkened in the image. As shown in a zoom-in image of an interface region in Figure 3b, the interfacial layer is only ≈0.5 nm thick. The sharp interface benefits from the excellent chemical stability of MAO substrates at high temperatures. In addition, STEM-EDS analysis using the *K*-series X-ray peaks of Mn and Pt elements yields an atomic ratio of $Mn_{45.2}Pt_{54.8}$ for the MnPt layer, which is in good agreement with the RBS and SEM-EDS measurements.

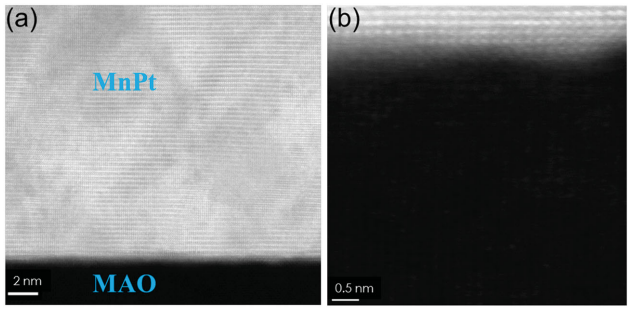

Figure 3. TEM characterization. a) Cross-sectional TEM image of an MnPt/MAO heterostructure. b) Zoom-in image of an interfacial region.

Magnetic properties of the MnPt/MAO films were examined by a Quantum Design SQUID. Surprisingly, all the as-deposited films exhibit large (relative to its AFM nature in bulk) room-temperature in-plane magnetization of ≈90 emu cc^{-1} and clear *M*–*H* hysteresis loops in the SQUID measurements (**Figure 4**a). Temperature-dependent magnetization measurements reveal a T_c of ≈400 K (Figure S1a, Supporting Information). As SQUID measurements collect complex signals from both thin films and substrates, we further performed PNR measurements on the time-of-flight magnetism reflectometer at the Spallation Neutron Source in Oak Ridge National Laboratory.[25] From the PNR experiments, spin asymmetry, SA, is obtained, which is defined as $SA = (R^+ - R^-)/(R^+ + R^-)$, where R^+ and R^- are reflectivity of polarized spin-up and spin-down neutron beams, respectively. When SA = 0, there is no magnetic moment in the system. Due to coexistent nuclear and magnetic scattering, PNR is capable of collecting structural and magnetic information at the same time.

A neutron beam with a wavelength band of 2–8 Å and a high polarization of 99%–98.5% was used. An external 1 T magnetic field was applied in-plane during measurements. PNR measurements reveal a sharp structural interface between the MnPt film and the MAO substrate over the whole lateral size of the sample (10×10 mm^2) with an average roughness of ≈0.2 nm. The PNR data are shown in Figure 4b and the according spin asymmetry is plotted in Figure S2 (Supporting Information). The fitted magnetization average over the entire film is ≈98 emu cc^{-1}, which is close to the SQUID value. Thus, the PNR measurements give direct conformational evidence that the observed ferromagnetism resides in the as-deposited MnPt film.

It was found that such ferromagnetism can be completely eliminated by postannealing at 800 °C in vacuum for 1 h. After annealing, the RHEED patterns of MnPt films remain relatively

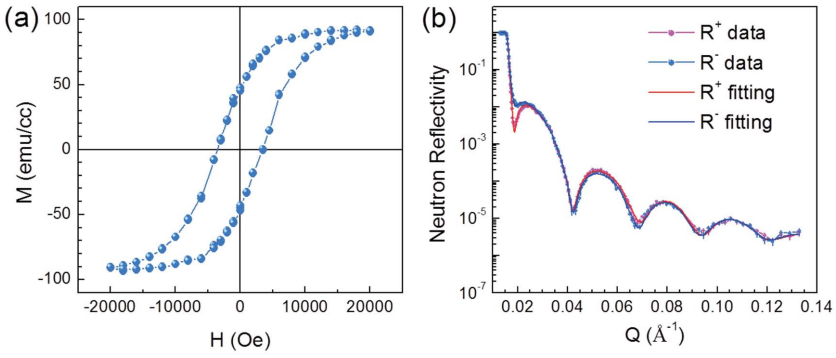

Figure 4. Ferromagnetism in as-deposited MnPt films. a) *M–H* loop measured by SQUID up to 2 T at 300 K. b) Neutron reflectivity spectra of two polarization states measured at 300 K under 1 T and the corresponding fitted curves. Error bars are marked on the data.

unchanged, suggesting a negligible effect of annealing on the surface condition. The compositions of annealed films were examined to be the same within the measurement error. Nevertheless, all the MnPt XRD peaks become stronger and sharper (**Figure 5**a), indicating the enhancement of chemical ordering and crystallinity. As a consequence, the magnetization becomes negligible in annealed films (Figure 5b). Although the temperature dependence of magnetization of annealed MnPt films is noisy owing to a tiny moment of the film, an AFM-like behavior can still be seen in Figure S1b (Supporting Information). Since it is difficult to measure a weak magnetic signal of a thin film grown on a bulk substrate by SQUID, element-specific X-ray magnetic circular dichroism (XMCD) was further performed on an annealed MnPt film at beamline 6.3.1 of the advanced light source with a grazing incidence angle of 30° and an in-plane magnetic field of 1.9 T. The characteristic Mn L_3 edge peak was specifically investigated, as shown in the X-ray absorption spectrum (Figure 5c). However, the XMCD signal is on the noise level (Figure 5d), indicating negligible magnetic moment, which is in accordance with the SQUID measurement results.

The electrical resistivity of both as-deposited and annealed MnPt films was measured as a function of temperature (ρ–T) from 300 to 2 K by a quantum design physical property measurement system. The measurement was performed in the four-probe linear geometry, and electrical contacts were made through wire bonding using Al wires. As plotted in Figure 5e,f, the MnPt resistivity has rather weak temperature dependence over the entire temperature range for both as-deposited and annealed films. The overall temperature coefficient of resistivity (TCR) is ≈110 ppm K^{-1} for an annealed film, which offers intriguing potential to serve as a low TCR metal alloy for precise electronic applications.[26] After annealing, the room-temperature resistivity reduces by 17%, which is consistent with the suppression of electron scattering from disorder as a result of enhanced crystallinity. The room-temperature resistivity of the annealed film is 136.6 μΩ cm, comparable to the bulk MnPt resistivity.[27] Intriguingly, a Kondo-like resistance

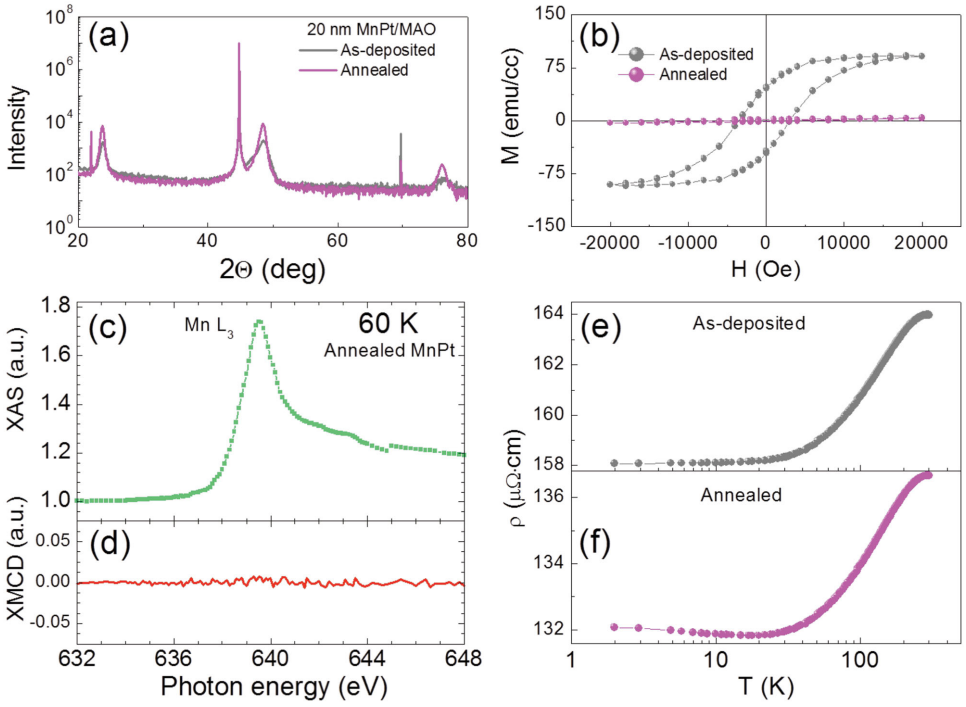

Figure 5. Annealed MnPt/MAO: structure, magnetism, and resistivity. a) θ–2θ scan of an annealed 20 nm thick MnPt/MAO film. The θ–2θ scan of an as-deposited film is plotted in gray for reference. b) Magnetization of the annealed MnPt film compared with that before annealing. c) Mn L_3 XAS and d) XMCD spectra of the annealed MnPt film measured at 60 K under an in-plane magnetic field of 1.9 T. Temperature-dependent resistivity of e) as-deposited and f) annealed MnPt films.

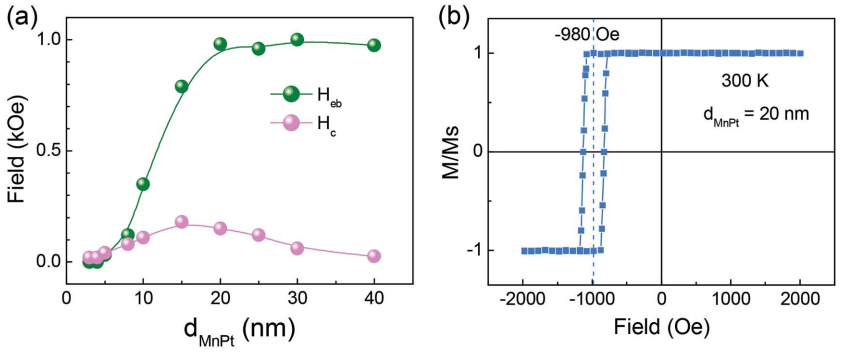

Figure 6. Exchange bias of AFM MnPt films with FM CoFe. a) Exchange bias field H_{eb} and coercivity field H_c as a function of MnPt thickness d_{MnPt} in Pt(2 nm)/CoFe(5 nm)/MnPt(d_{MnPt})/MAO structures. b) *M*–*H* loop of a Pt(2 nm)/CoFe(5 nm)/MnPt(20 nm)/MAO structure measured at 300 K.

minimum shows up at ≈18 K, reminiscent of the fact that the Kondo effect typically appears in spin systems without macroscopic magnetic moment.[28]

These experimental facts suggest that the novel ferromagnetism in as-deposited MnPt films is related to defects. As the magnetic order in the Mn–Pt alloy system is dominated by exchange interactions between nearest neighbor Mn atoms,[7] Mn-related defects can affect the magnetic order in the system. The defect-induced ferromagnetism in electron systems without any magnetic order in their pristine phase is widely observed in strongly correlated 3d metal oxides.[29–31] Additionally, defect-enhanced ferromagnetism has been recently manifested in FM metal alloys as well.[32] Nevertheless, the emergence of ferromagnetism in an AFM matrix is rather intriguing.

We therefore performed systematic density functional theory based first-principle calculations (Figure S3, Supporting Information). By considering Figure S3a,b of Supporting Information, we conclude that the predicted energy jump range due to the spin-flipping stabilized by Mn/Pt antisites in the FM state is in line with the aforementioned experimental observations: the FM state in MnPt films grown at 600 °C and the AFM state in MnPt film postannealed at 800 °C. That is because upon annealing Mn/Pt antisites are corrected, and thus the spin-flipping of Mn atoms is removed. The embedded mechanism is that the appearance of FM1 makes the FM state more stable compared to the AFM state, while the appearance of FM2 makes the AFM state more stable.

To examine the exchange coupling between an optimized AFM MnPt film and a ferromagnetic layer, a 5 nm $Co_{0.9}Fe_{0.1}$ (CoFe) film and a 2 nm Pt capping layer were deposited on top of MnPt at room temperature, where the MnPt thickness d_{MnPt} was systematically varied from 3 to 40 nm, i.e., Pt(2 nm)/CoFe(5 nm)/MnPt(d_{MnPt})/MAO. Magnetic measurements performed in a Quantum Design SQUID at 300 K reveal an exchange bias effect for $d_{MnPt} > 4$ nm. The exchange bias field H_{eb} rapidly increases with d_{MnPt} between 8 and 20 nm and then saturates (**Figure 6**a). As shown in Figure 6b, the in-plane *M*–*H* loop of an exchange system with a 20 nm thick MnPt measured from 2000 → –2000 → 2000 Oe entirely shifts to the negative side. The coercivity field is ≈150 Oe, which is much larger than the coercivity field of a noncoupled CoFe film (≈20 Oe). H_{eb} is ≈980 Oe, more than twice the largest H_{eb} in the CoFe/MnPt system[18] and other FM/MnPt systems based on polycrystalline MnPt films fabricated at low temperatures.[17] This demonstrates the critical role of chemical ordering of AFM MnPt in enhancing exchange coupling. Another striking feature in the exchange bias effect is that the magnetic switching of CoFe magnetization is rather sharp, stating homogeneous exchange coupling strength over the monolithic MnPt film. The large exchange bias at room temperature implies that the surface layer of the AFM MnPt film has an uncompensated in-plane spin moment, suggesting a possible surface spin rearrangement in single crystalline MnPt films.

In summary, we have achieved high-quality MnPt films epitaxially grown on MAO, which demonstrates the feasibility of epitaxial integration of magnetic metal alloys with oxides as long as selected oxides are both chemically and structurally compatible with metal alloys. In addition, highly chemically ordered and single-crystalline MnPt films with the AFM order show superiorly strong exchange coupling with a ferromagnetic layer, which is attractive for spintronic device applications. Magnetic properties of MnPt thin films were explored to be sensitive to spin-flipping of Mn atoms stabilized by Mn/Pt antisites. This indeed provides a novel path to realizing ferromagnetism in an even rather robust AFM intermetallic alloy. Moreover, high-quality epitaxial films grown on insulating oxides enable AFM spintronic studies on MnPt as well.

Supporting Information

Supporting Information is available from the Wiley Online Library or from the author.

Acknowledgements

The authors dedicate this work to the memory of our friend and collaborator, Dr. Michael Biegalski. We acknowledge Prof. R. Ramesh (U.C. Berkeley) for continued advice and Prof. J. M. D. Coey (Trinity College, Ireland) and for illuminating discussions. Dr. X Renshaw Wang is acknowledged for help with the illustrations. This work (Z.L.) was sponsored by the Laboratory Directed Research and Development (LDRD) Program of ORNL managed by UT-Battelle, LLC; by the US Department of Energy (DOE), Office of Science, Basic Energy Sciences, Materials Sciences and Engineering Division (L.L., A.S.S., T.Z.W., H.N.L., J.A.N., K.W., and T.L.M.); and under US DOE grant DE-SC0002136 (A.T.W.). S.S, C.M., and Z.L. thank the support from the Natural Science Foundation (NSF) with Grant Nos. CHE-1230924 and CMMI-1333999. First-principle calculations were carried out using NERSC resources supported by the DOE Office of Science under contract No. DE-AC02-05CH11231. Part of the work was performed at ORNL's Center for Nanophase Materials Sciences, and the Spallation Neutron Source, which are DOE Office of Science User Facilities. The Advanced Light Source is supported by the Director, Office of Science, Office of Basic Energy Sciences, of the U.S. Department of Energy under Contract No. DE-AC02-05CH11231.

Received: June 1, 2015
Revised: October 4, 2015
Published online: November 5, 2015

[1] R. Ramesh, N. A. Spaldin, *Nat. Mater.* **2007**, *6*, 21.
[2] R. O. Cherifi, V. Ivanovskaya, L. C. Phillips, A. Zobelli, I. C. Infante, E. Jacquet, V. Garcia, S. Fusil, P. R. Briddon, N. Guiblin, A. Mougin, A. A. Ünal, F. Kronast, S. Valencia, B. Dkhil, A. Barthélémy, M. Bibes, *Nat. Mater.* **2014**, *13*, 345.
[3] Y. Lee, Z. Q. Liu, J. T. Heron, J. D. Clarkson, J. Hong, C. Ko, M. D. Biegalski, U. Aschauer, S. L. Hsu, M. E. Nowakowski, J. Wu, H. M. Christen, S. Salahuddin, J. B. Bokor, N. A. Spaldin, D. G. Schlom, R. Ramesh, *Nat. Commun.* **2015**, *6*, 5959.
[4] W. Eerenstein, M. Wiora, J. L. Prieto, J. F. Scott, N. D. Mathur, *Nat. Mater.* **2007**, *6*, 348.
[5] S. Zhang, Y. G. Zhao, P. S. Li, J. J. Yang, S. Rizwan, J. X. Zhang, J. Seidel, T. L. Qu, Y. J. Yang, Z. L. Luo, Q. He, T. Zou, Q. P. Chen, J. W. Wang, L. F. Yang, Y. Sun, Y. Z. Wu, X. Xiao, X. F. Jin, J. Huang, C. Gao, X. F. Han, R. Ramesh, *Phys. Rev. Lett.* **2012**, *108*, 137203.
[6] L. Pál, E. Krén, G. Kádár, P. Szabó, T. Tarnóczi, *J. Appl. Phys.* **1968**, *39*, 538.
[7] E. Kren, G. Kadar, L. Pal, J. Solyom, P. Szabo, T. Tarnoczi, *Phys. Rev.* **1968**, *171*, 574.
[8] H. Hama, R. Motomura, T. Shinozaki, Y. Tsunoda, *J. Phys. Condens. Matter* **2007**, *19*, 176228.
[9] A. B. Shick, S. Khmelevskyi, O. N. Mryasov, J. Wunderlich, T. Jungwirth, *Phys. Rev. B* **2010**, *81*, 212409.
[10] B. G. Park, J. Wunderlich, X. Martí, V. Holý, Y. Kurosaki, M. Yamada, H. Yamamoto, A. Nishide, J. Hayakawa, H. Takahashi, A. B. Shick, T. Jungwirth, *Nat. Mater.* **2011**, *10*, 347.
[11] X. Martí, B. G. Park, J. Wunderlich, H. Reichlová, Y. Kurosaki, M. Yamada, H. Yamamoto, A. Nishide, J. Hayakawa, H. Takahashi, T. Jungwirth, *Phys. Rev. Lett.* **2012**, *108*, 017201.
[12] D. Petti, E. Albisetti, H. Reichlová, J. Gazquez, M. Varela, M. Molina-Ruiz, A. F. Lopeandía, K. Olejník, V. Novák, I. Fina, B. Dkhil, J. Hayakawa, X. Marti, J. Wunderlich, T. Jungwirth, R. Bertacco, *Appl. Phys. Lett.* **2013**, *102*, 192404.
[13] Y. Y. Wang, C. Song, B. Cui, G. Y. Wang, F. Zeng, F. Pan, *Phys. Rev. Lett.* **2012**, *109*, 137201.
[14] X. Marti, I. Fina, C. Frontera, J. Liu, P. Wadley, Q. He, R. J. Paull, J. D. Clarkson, J. Kudrnovský, I. Turek, J. Kuneš, D. Yi, J. Chu, C. T. Nelson, L. You, E. Arenholz, S. Salahuddin, J. Fontcuberta, T. Jungwirth, R. Ramesh, *Nat. Mater.* **2014**, *13*, 367.
[15] R. F. C. Farrow, R. F. Marks, S. Gider, A. C. Marley, S. Parkin, D. Mauri, *J. Appl. Phys.* **1997**, *81*, 4986.
[16] J. P. Nozières, S. Jaren, Y. B. Zhang, A. Zeltser, K. Pentek, V. S. Speriosu, *J. Appl. Phys.* **2000**, *87*, 3920.
[17] M. F. Toney, M. G. Samant, T. Lin, D. Mauri, *Appl. Phys. Lett.* **2002**, *81*, 4565.
[18] M. Rickart, P. P. Freitas, I. G. Trindade, N. P. Barradas, E. Alves, M. Salgueiro, N. Muga, J. Ventura, J. B. Sousa, G. Proudfoot, D. Pearson, M. Davis, *J. Appl. Phys.* **2004**, *95*, 6317.
[19] M. M. Soares, M. De Santis, H. C. N. Tolentino, A. Y. Ramos, M. El Jawad, Y. Gauthier, F. Yildiz, M. Przybylski, *Phys. Rev. B* **2012**, *85*, 1.
[20] W. D. Nix, *Metall. Trans. A* **1989**, *20A*, 2217.
[21] O. Saburi, *J. Phys. Soc. Japan* **1959**, *14*, 1159.
[22] Z. Q. Liu, D. P. Leusink, X. Wang, W. M. Lu, K. Gopinadhan, A. Annadi, Y. L. Zhao, X. H. Huang, S. W. Zeng, Z. Huang, A. Srivastava, S. Dhar, T. Venkatesan, Ariando, *Phys. Rev. Lett.* **2011**, *107*, 146802.
[23] Z. Q. Liu, C. J. Li, W. M. Lü, X. H. Huang, Z. Huang, S. W. Zeng, X. P. Qiu, L. S. Huang, A. Annadi, J. S. Chen, J. M. D. Coey, T. Venkatesan, *Phys. Rev. X* **2013**, *3*, 021010.
[24] J. Schubert, O. Trithaveesak, A. Petraru, C. L. Jia, R. Uecker, P. Reiche, D. G. Schlom, *Appl. Phys. Lett.* **2003**, *82*, 3460.
[25] V. Lauter, H. Ambaye, R. Goyette, W. T. H. Lee, A. Parizzi, *Physica B* **2009**, *404*, 2543.
[26] S. K. Chen, Y. F. Kao, *AIP Adv.* **2012**, *2*, 012111.
[27] R. Y. Umetsu, K. Fukamichi, A. Sakuma, *Mater. Trans.* **2006**, *47*, 2.
[28] P. Nozières, A. Blandin, *J. Phys.* **1980**, *41*, 193.
[29] J. M. D. Coey, P. Stamenov, R. D. Gunning, M. Venkatesan, K. Paul, *New J. Phys.* **2010**, *12*, 053025.
[30] Z. Q. Liu, W. M. Lü, S. L. Lim, X. P. Qiu, N. N. Bao, M. Motapothula, J. B. Yi, M. Yang, S. Dhar, T. Venkatesan, Ariando, *Phys. Rev. B: Condens. Matter* **2013**, *87*, 220405(R).
[31] Z. Q. Liu, W. Lu, S. W. Zeng, J. W. Deng, Z. Huang, C. J. Li, M. Motapothula, W. M. Lü, L. Sun, K. Han, J. Q. Zhong, P. Yang, N. N. Bao, W. Chen, J. S. Chen, Y. P. Feng, J. M. D. Coey, T. Venkatesan, *Adv. Mater. Interfaces* **2014**, *1*, 1400155.
[32] Y. Murakami, K. Niitsu, T. Tanigaki, R. Kainuma, H. S. Park, D. Shindo, *Nat. Commun.* **2014**, *5*, 4133.